Efficient Analysis of Periodic Dielectric Waveguides using Dirichlet-to-Neumann Maps

Johannes Tausch and Jerome Butler

SMU Math Report 2001-01

Department of Mathematics
Southern Methodist University

Efficient Analysis of Periodic Dielectric Waveguides using Dirichlet-to-Neumann Maps

Johannes Tausch
Southern Methodist University
Department of Mathematics
Dallas, TX 75275
tausch@mail.smu.edu

Jerome Butler
Southern Methodist University
School of Engineering and Applied Science
Dallas, TX 75275
jkb@smu.edu

Abstract

We present a numerical scheme for the analysis of periodic dielectric waveguides using Floquet-Bloch theory. The problem of finding the fundamental propagation modes is reduced to a nonlinear eigenvalue problem involving Dirichlet-to-Neumann maps. This approach leads to much smaller matrix problems than the ones that have appeared previously. By increasing the discretization fineness any desired precision of the method can be achieved. We discuss an eigensolver and extend the conventional rule to choose the branches of the transverse wave numbers. This ensures analytic dependence on the Floquet multiplier and convergence of the nonlinear solver. We will demonstrate that even for a complicated multilayer waveguide structure the propagation factors can be calculated within seconds to several digits of accuracy.

1 Introduction

Many integrated optics devices, such as waveguide couplers, microwave filters or DFB structures, contain dielectric waveguides with periodic corrugations. It is typical for these devices that the guided wavelength is of the same order as the spatial period and hence it is necessary to apply field theory to analyze their characteristic propagation modes.

The form of electromagnetic waves traveling along periodic structures is described by Floquet's Theorem, which states that the field $\mathbf{\Psi}$ of a characteristic mode in a z-periodic structure is of the form

$$\mathbf{\Psi}(x, y, z) = \exp(\gamma z)\mathbf{\Phi}(x, y, z), \tag{1}$$

where $\mathbf{\Phi}$ is a z-periodic vector valued function and γ is the propagation constant. The real part of γ represents the attenuation and the imaginary part the phase shift of the fundamental mode in one period.

In the design of integrated optics devices there are many situations where the possible propagation constants are unknown and need to be determined numerically. The propagation constants of interest are usually those that correspond to guided or almost guided modes which means that the real part is usually by orders of magnitude smaller than the imaginary part. If a reasonable approximation of the attenuation is sought, it is necessary to resolve the propagation constant to many digits of accuracy. This necessitates very fine discretizations and dealing with very large matrix problems. Often, this must be accomplished for a wide rage of frequencies. Therefore fast and robust numerical algorithms are extremely important to enable the development of optics devices interactively on a computer.

Although the quantitative behavior of the Floquet spectrum of axially periodic multilayered structures is well understood [1, 2], finding good numerical schemes is still a topic of current research.

A variety of computer-based techniques have been suggested for dielectric gratings in integrated-optics devices. Most methods deal with scattering and refraction-type problems, such as [3, 4, 5, 6, 7, 8, 9, 10, 11, 12], but some of these methods have also been modified to deal with guiding problems. The common feature is that they are based of a discretization of the Helmholtz equation in the grating layer which is coupled with the solution in the uniform layers. The difference is mainly in the the way the problem in the grating layer is treated. For instance, the solution has been expanded by complex exponentials [13], or, more recently, treated with a boundary element technique (BEM) [14, 15]. These approaches result in a large matrix whose size is given by the number of degrees of freedom of the discretization for the grating and the uniform layers. Since some of the matrix coefficients depend in a highly nonlinear fashion on the propagation constant γ, the discretized problem is a nonlinear eigenvalue problem, i.e., the value of γ must be determined that makes the discretized system singular.

Almost all contemporary approaches to find the propagation constant rely on finding the roots of the determinant with Muller's method. This is

preferred over Newton's method because no derivatives must be evaluated. However, the numerical cost can be high when fine discretizations are employed. Furthermore, the nonlinear solver can be slow, or may not converge at all, if no good initial guess of the propagation constant is known.

The method described in this paper relies on finding the roots of a Dirichlet-to-Neumann operator. Since this problem is posed on two line segments and not, as the approaches mentioned above, on a two-dimensional domain, the benefit is that a much smaller nonlinear eigenvalue problem must be solved, even if a very fine discretization is used.

We will also devise a new iterative solver for the eigenvalue problem, which is based on the linearization of the matrix problem, and not of the determinant, as the previous approaches.

One of the fundamental questions in the analysis of dielectric periodic waveguides is the branch choice for the transverse wave numbers in the super- and substrate regions. We will show in the appendix how to extend the usual rule to the case of propagation factors with positive real part. This is necessary to ensure analytic dependence of γ and convergence of the nonlinear solver in the neighborhood of guided modes. A non-analytic extension will lead to lead to non-convergence of the solver in many cases.

2 Mathematical Formulation

A typical waveguide geometry is shown in Figure 1. It consists of a substrate region, several stratified layers, a small grating layer, that can be sandwiched between the stratified layers, and a superstrate region. The different layers are denoted by Ω_j, $j = 0, \ldots, J$. The super- and substrate regions, Ω_0 and Ω_J, respectively, have infinite extend. The structure is infinite and homogeneous in y-direction. We assume the layers are linear, isotropic and non-dispersive, and therefore the magnetic permeability μ and the electric permittivity ϵ are constant scalars in each layer. A finite conductivity of the material can be accounted for by letting ϵ be complex.

This is a suitable geometry for practical devices because the contemporary epitaxial crystal growth produces layers that are piecewise continuous for the constitutive parameters. Further, the gratings are fabricated by producing a periodic structure on a top layer after growth. The layer above the grating may be air or another epitaxial layer.

For this geometry the fundamental modes of the guide are either transverse electric, i.e., the electric field has the form $\mathbf{E}(x, y, z) = u(x, z)\,\mathbf{e}_y$, or transverse magnetic, i.e., the magnetic field has the form $\mathbf{H}(x, y, z) =$

$u(x,z)\,\mathbf{e}_y$. In both cases, the wave function u satisfies the Helmholtz equation

$$\Delta u + \mu\epsilon\omega^2 u = 0, \tag{2}$$

in each layer, where time harmonic variation is assumed. Depending on the polarization of the mode, the conditions

$$u^+ = u^- \quad \text{and} \quad \frac{1}{\mu^+}\frac{\partial u^+}{\partial n} = \frac{1}{\mu^-}\frac{\partial u^-}{\partial n} \qquad \text{for TE modes,} \tag{3}$$

$$u^+ = u^- \quad \text{and} \quad \frac{1}{\epsilon^+}\frac{\partial u^+}{\partial n} = \frac{1}{\epsilon^-}\frac{\partial u^-}{\partial n} \qquad \text{for TM modes} \tag{4}$$

hold at the interface of two different layers. Here the superscripts refer to the positive or negative side of the interface. In most practical optical waveguiding systems the material is non-magnetic and the magnetic permeablity is that of free space.

By Floquet's Theorem, the fundamental modes must satisfy the periodic condition

$$u(x, z+\Lambda) = \exp(\gamma\Lambda)u(x,z)\,, \tag{5}$$

where the number γ is the propagation constant, which, in general, is complex. Because of this condition, the Helmholtz equation can be solved in one fundamental period of the grating, which is an infinite strip of width Λ. The boundary conditions on the upper and lower edge, Γ_0 and Γ_2, respectively, are

$$u|_{\Gamma_2} = \exp(\gamma\Lambda)\, u|_{\Gamma_0} \quad \text{and} \quad \left.\frac{\partial u}{\partial n}\right|_{\Gamma_2} = -\exp(\gamma\Lambda)\left.\frac{\partial u}{\partial n}\right|_{\Gamma_0}. \tag{6}$$

The negative sign in the last equation is necessary because the normals on Γ_0 and Γ_2 are oriented in opposite directions.

In order to treat the Helmholtz equation numerically, we decompose the infinite strip in a finite (interior) region Ω_{int}, that contains the grating layer and two exterior semi-infinite domains Ω_+ and Ω_- where the materials are assumed to be constant; see Figure 2. The interfaces of the domains are denoted by Γ_3, where Γ_3^- is the left and Γ_3^+ the right interface.

For numerical efficiency of the method it is desirable to include stratified layers in the exterior domains. We will describe the alteration of the method for this situation in Section 2.2.

The core of the method described below is that the problem in the interior region is solved numerically and matched with the analytical solution in the exterior regions. A propagation factor is a value of γ for which a nontrivial solution in the three regions can be extended to a solution on

the infinite strip. In [16] we showed that this is a necessary and sufficient condition to obtain all propagation factors.

The solution in the exterior regions can be expanded in terms of space harmonics in the form

$$u(x,z) = \sum_{n\in\mathbf{Z}} f_n^- \exp\left(ik_{xn}^J(x-x^+)\right)\exp(k_{zn}z), \quad x \geq x^+ \tag{7}$$

$$u(x,z) = \sum_{n\in\mathbf{Z}} f_n^+ \exp\left(ik_{xn}^0(x^- - x)\right)\exp(k_{zn}z), \quad x \leq x^- \tag{8}$$

where $i=\sqrt{-1}$, $j \in \{0, J\}$ and

$$k_{zn} = \frac{2\pi i n}{\Lambda} + \gamma, \tag{9}$$

$$k_{xn}^j = \pm\sqrt{k_{zn}^2 + \mu_j\epsilon_j\omega^2}\,. \tag{10}$$

Throughout this article the square root has the branch cut on the negative real axis, i.e., the function values have non-negative real part. The choice of the sign in (10) will be discussed in the appendix. The $f_n^\pm$'s are the Fourier coefficients of the solution on $\Gamma_3^\pm$

$$f_n^\pm = \frac{1}{\Lambda}\int_0^\Lambda u(x^\pm, z)\,\exp(-k_{zn}z)\,dz. \tag{11}$$

If γ and u on the interfaces Γ_3 are given, the solution in the exterior regions as well as the normal derivative $\frac{\partial u}{\partial n}$ on Γ_3 can be obtained from (11), (7) and (8). The mapping from $u|_{\Gamma_3}$ to $\frac{\partial u}{\partial n}\Big|_{\Gamma_3}$ is the Dirichlet-to-Neumann (DtN) map for the exterior region, which we symbolically write as

$$\left.\frac{\partial u}{\partial n}\right|_{\Gamma_3} := T_{\text{ext}}(\gamma)u|_{\Gamma_3} = \begin{cases} \sum_{n\in\mathbf{Z}} ik_{xn}^J f_n^+ \exp(k_{zn}z) & \text{on } \Gamma_3^+ \\ \sum_{n\in\mathbf{Z}} ik_{xn}^0 f_n^- \exp(k_{zn}z) & \text{on } \Gamma_3^- \end{cases} \tag{12}$$

If Γ_3 does not coincide with a material interface, u and its normal derivative must be continuous across Γ_3 to obtain a solution on the infinite strip. This gives the boundary condition on Γ_3 for the interior problem

$$\left.\frac{\partial u^-}{\partial n}\right|_{\Gamma_3} = T_{\text{ext}}(\gamma)u|_{\Gamma_3}\,. \tag{13}$$

Thus we see that the problem of finding the propagation factors reduces

to finding the values of γ for which the Helmholtz equation in Ω_{int}

$$\begin{aligned} \Delta u + \mu\epsilon\omega^2 u &= 0, \quad \text{in } \Omega_{int} \\ u|_{\Gamma_2} &= \exp(\gamma\Lambda)\, u|_{\Gamma_0} \\ \left.\frac{\partial u}{\partial n}\right|_{\Gamma_2} &= -\exp(\gamma\Lambda)\, \left.\frac{\partial u}{\partial n}\right|_{\Gamma_0} \\ \left.\frac{\partial u}{\partial n}\right|_{\Gamma_3} &= T_{\text{ext}}(\gamma) u|_{\Gamma_3}\,. \end{aligned} \tag{14}$$

has nontrivial solutions.

Formulation (14) is suitable for numerical computations because only a finite domain must be discretized. This can be done either with the finite element method or the boundary element method. Both approaches are standard for the 2-D Helmholtz equation and we do not discuss the details here, rather refer to standard texts, such as [17].

After discretization the Helmholtz equation is reduced to a linear system of which some coefficients depend in a non-linear fashion on the propagation constant γ. The task is to find γ such that the matrix is non-singular, which is a non-linear eigenvalue problem.

Previous approaches are based on discretizations of this boundary value problem. These methods differ in the solution method of the interior problem; for instance, [13] describes an expansion in spatial harmonics, and [14] describes the use of the boundary element method.

We do not follow this development. Rather we introduce in the following an equivalent formulation which will lead to much smaller matrix problems. For that consider the interior DtN map. We assume that the given value of γ is such that the Helmholtz equation in Ω_{int} with given Dirichlet boundary conditions on Γ_3

$$\begin{aligned} \Delta u + \mu\epsilon\omega^2 u &= 0, \quad \text{in } \Omega_{int} \\ u|_{\Gamma_2} &= \exp(\gamma\Lambda)\, u|_{\Gamma_0} \\ \left.\frac{\partial u}{\partial n}\right|_{\Gamma_2} &= -\exp(\gamma\Lambda)\, \left.\frac{\partial u}{\partial n}\right|_{\Gamma_0} \\ u|_{\Gamma_3} &= f \end{aligned} \tag{15}$$

has a unique solution u. Then the interior DtN map is given by

$$T_{\text{int}}(\gamma) f := \left.\frac{\partial u}{\partial n}\right|_{\Gamma_3}, \tag{16}$$

where u is the solution of (15).

The propagation constants are exactly the values of γ that make the operator

$$T(\gamma) := T_{\text{int}}(\gamma) - T_{\text{ext}}(\gamma) \tag{17}$$

singular. That is, there is a Dirichlet condition $f \neq 0$ on Γ_3 such that

$$T(\gamma) f = 0\,. \tag{18}$$

To understand why it suffices to solve (18), recall that the Dirichlet data extend to a solution u of the interior and exterior Helmholtz equations. Since f is in the nullspace of $T(\gamma)$, the normal derivatives approached from both sides of the interfaces Γ_3 match, and therefore u is a solution on the infinite strip. Hence u is a non-trivial solution of the Helmholtz equation and γ is a propagation constant.

Problem (18) is attractive for numerical calculation because the unknown f is defined only on the interface Γ_3. Thus much fewer degrees of freedom in the discretization are required than the problem in Ω_{int}.

2.1 Discretization of the DtN map

To discretize operator equation (18) a Galerkin approach is employed. To this end, write the approximate solution as a linear combination of harmonics up to a given degree p

$$f_p = \sum_{|n|\leq p} f_n^+ e_n^+ + \sum_{|n|\leq p} f_n^- e_n^- \tag{19}$$

where

$$e_n^\pm(z) := \begin{cases} \exp\left(k_{zn} z\right), & \text{on } \Gamma_3^\pm, \\ 0, & \text{on } \Gamma_3^\mp, \end{cases} \tag{20}$$

We seek a propagation constant γ_p and a non-zero function f_p of the form of (19) such that the residual $T(\gamma_p) f_p$ is orthogonal to the functions $e_n^\pm$ for $|n| \leq p$. This results in the non-linear eigenvalue problem

$$T_p(\gamma_p) f_p = 0\,, \tag{21}$$

where $T_p(\gamma_p)$ is a matrix of size $4p+2$ whose coefficients depend nonlinearly on γ.

In view of (17), the coefficients of $T_p(\gamma_p)$ are the difference of the discretized interior and exterior DtN maps. It follows from (12) and the orthogonality of the harmonics that the exterior discretized DtN map is a diagonal matrix of size $4p+2$ with entries ik_{xn}^0 and ik_{xn}^J.

In the interior region coupling of modes occurs and thus the discretization of the interior DtN map is a dense matrix. To obtain the columns of this matrix, the interior problems (15) with the Dirichlet condition

$$f = e_n^\pm \tag{22}$$

on $\Gamma_3^{\pm}$ must be solved $4p+2$ times for all harmonics in (20). The matrix entries of $T_{\mathrm{int},p}(\gamma)$ are the Fourier coefficients of the normal derivative of the solutions of (15) with the boundary condition on Γ_3 given by (22), that is,

$$[T_{\mathrm{int},p}(\gamma)]_{n\pm,m\pm} = \int_0^{\Lambda} e_n^{\pm}(z) \left.\frac{\partial \bar{u}_m}{\partial n_z}\right|_{\Gamma_3^{\pm}} dz. \tag{23}$$

The interior problem (15) has no closed solution and therefore a second discretization is required to obtain the normal derivatives of the field in (23). This can be accomplished with a finite element discretization as we have demonstrated [16], but more recently we have utilized the BEM which has proved to be more efficient. For a detailed description of the BEM in the context of dielectric waveguides we refer to, e.g., [14].

Since the BEM has only unknowns on the interfaces $\Gamma_0, \Gamma_1, \Gamma_2$ and Γ_3, the resulting influence matrix is small enough to be handled with direct methods as opposed to iterative methods which are much more expensive for small problems. To solve the $4p+2$ interior problems the influence matrix and its LU decomposition have to be computed only once. Thus the overall computational cost does not significantly increase with p.

Once a solution of (21) has been determined, the eigenmode can be calculated in the exterior regions by (7) and in the interior region by using Green's formula.

2.2 Including uniform layers in the exterior problem

Since the interior problem must be solved repeatedly for each step of the nonlinear solver, it is important for the efficiency of the method that the interior domain Ω_{int} is kept as small as possible. This can be achieved by including the uniform layers in the exterior domains Ω_+ and Ω_-. To account for these layers, the exterior DtN map must be modified using a transfer matrix analysis.

We first describe this for a TE mode. In this case, the j-th finite stratified layer is of the form

$$u(x,z) = \sum_{n\in\mathbf{Z}} \exp(k_{zn}z) \left\{ \cos(k_{xn}^j(x-x_j))\phi_n^j + \frac{\mu_j}{k_{xn}^j} \sin(k_{xn}^j(x-x_j))\psi_n^j \right\}. \tag{24}$$

Here, the state variables ϕ_n^j and ψ_n^j describe the function value and the derivative at the interfaces of the layers and are given by

$$\phi_n^j \;=\; u_n(x_j), \tag{25}$$

$$\psi_n^j \;=\; \frac{1}{\mu_j}\frac{\partial u_n}{\partial x}(x_j), \tag{26}$$

where the u_n's are the Fourier coefficients of u. Because of the interface conditions on u in (3), the state variables of two adjacent layers are coupled via the relation

$$\begin{bmatrix} \phi_n^{j+1} \\ \psi_n^{j+1} \end{bmatrix} = T_n^j(\gamma) \begin{bmatrix} \phi_n^j \\ \psi_n^j \end{bmatrix}, \tag{27}$$

where the matrix $T_n^j(\gamma)$ is the transfer of the state variables across layer j

$$T_n^j(\gamma) = \begin{bmatrix} 1 & 0 \\ 0 & \frac{1}{\mu_j} \end{bmatrix} \begin{bmatrix} \cos(k_{xn}^j w_j) & \sin(k_{xn}^j w_j)/k_{xn}^j \\ -\sin(k_{xn}^j w_j) k_{xn}^j & \cos(k_{xn}^j w_j) \end{bmatrix} \begin{bmatrix} 1 & 0 \\ 0 & \mu_j \end{bmatrix}, \tag{28}$$

and w_j is the width of the jth layer.

The translation of the state variables from the outer- to the innermost layer (i.e., the interface Γ_3^- located at x_{j^-}) is the product of the translation operators across all layers

$$\begin{bmatrix} \phi_k^{j^-} \\ \psi_k^{j^-} \end{bmatrix} = T_n^{j^-}(\gamma) \cdot \ldots \cdot T_n^1(\gamma) \begin{bmatrix} 1 \\ k_{xn}^0 \end{bmatrix}. \tag{29}$$

The translation to the interface Γ_3^+ located at x_{j^+} follows in a similar fashion. The DtN maps at Γ_3 are then given by

$$T_{\text{ext}}(\gamma)\, e_n^{\pm} = \mu_j \frac{\psi_n^{j^\pm}}{\phi_n^{j^\pm}}\, e_n^{\pm}. \tag{30}$$

The exterior DtN map for a TM mode can be obtained by replacing the μ's in formulas (24-30) by ϵ's.

3 Nonlinear Solver

In this section we discuss a modification of Newton's method for the solution of the nonlinear eigenvalue problem (21). An obvious approach is to find the roots of the determinant of $T_p(\gamma)$ or to find the roots of the function

$$F(\mathbf{x}, \gamma) = \begin{bmatrix} T_p(\gamma)\mathbf{x} \\ \mathbf{x}^*\mathbf{x} - 1 \end{bmatrix} \tag{31}$$

with either Newton's or Muller's method. Although both ideas have been considered, see, e.g., [18] and the references therein, they have their own

difficulties for the particular application considered here. The determinant has large variations in γ which can cause an iterative solver to converge to a non-physical root. A solver based on setting $F(\mathbf{x}, \gamma) = 0$ requires in addition to the propagation constant a good initial guess for the eigenvector $\mathbf{x}$; this hard near Bragg conditions where solution branches intersect or nearly intersect. In that case, both solution techniques will converge only in a small neighborhood of the root.

The nonlinear solver used in this paper (later on referred to as the matrix-Newton method) has unique advantages associated with its convergence. The idea is to determine the correction of the current approximation $\bar{\gamma}$ (where T_p is nonsingular) such that the linearization of $T_p(\bar{\gamma} + \delta)$ becomes singular. By linearizing about $\bar{\gamma}$

$$T_p(\bar{\gamma}) + \delta T_p'(\bar{\gamma}) = \delta T_p(\bar{\gamma}) \left(\frac{1}{\delta} I + T_p(\bar{\gamma})^{-1} T_p'(\bar{\gamma}) \right) \tag{32}$$

the Newton correction can be determined from the largest eigenvalue λ of $T_p(\bar{\gamma})^{-1} T_p'(\bar{\gamma})$. The next iterate is then given by $\bar{\gamma} := \bar{\gamma} - 1/\lambda$.

Since discretizations typically require only a small value of p, the additional numerical cost for solving the eigenvalue problem for each linearization is insignificant compared to the cost of setting up the matrix $T_p(\gamma)$.

4 Numerical Results

In this section we include two example waveguides to demonstrate the efficiency and accuracy of the approach discussed. The first example is a simple waveguide with a rectangular corrugation. It has frequently appeared in the literature and serves us as a benchmark problem [15]. The second structure consists of two different guides with a grating layer sandwiched in between. The coupling of modes induced by the grating can lead to a power transfer between the guides. This combination of waveguides is an an example of a grating-assisted directional coupler (GADC) and has previously been discussed in [19]. Here we use this device to illustrate the feasibility of the DtN-approach to complicated structures. For both examples we calculate TE modes, where the magnetic permeability is that of free space; the values of the electric permittivity along with dimensions of the layers are listed in Tables 1 and 2.

Tables 3 and 4 and Figures 7-9 display the calculated propagation factor and the corresponding solution times for increasing the value of p in (21) and for decreasing the meshwidth h of the discretization of the interior

problem (15). The calculated propagation constant computed by Chang et. al. [3] is $\gamma/\omega = -1.8743 \times 10^{-2} + 1.5809i$. For our results, the interior solution is based on a boundary element discretization using piecewise constant elements. This turned out to be more efficient and more accurate than a finite element solution. From the tables it is clear that if p is increased, h must be decreased to obtain convergence of the calculated propagation factor, but even very coarse discretizations lead to good approximations of $\mathrm{Re}(\gamma)$. However, since $\mathrm{Re}(\gamma)$ is several orders of magnitudes smaller than $\mathrm{Im}(\gamma)$, a reasonably fine discretization is required to resolve the attenuation to a few digits of accuracy. In our example the values $p = 2$ and $h = 1/32$ were sufficient to determine the first two digits of $\mathrm{Im}(\gamma)$ and the first four digits of $\mathrm{Re}(\gamma)$, at a cpu time of about one second on a DEC alpha 500au workstation.

From Table 4 it follows that the computation time depends in a much larger extend on h than on p. The reason is that the size of a discretized interor problem is much larger than the size of the nonlinear eigenproblem $T_p(\gamma)$. Therefore, the cost an eigenvalue problem is negligible compared to solving an interior problem. This is the main reason why the matrix-Newton solver is more efficient than the more standard solvers based on (31).

Rapid calculations for a single frequency are extremely important because it always takes some experimentation with the initial guess for the nonlinear solver to get convergence to a mode near the imaginary axis. Random initial guesses usually result in convergence to non-physical leaky modes, but it is always possible to start the iteration with the propagation constant of an approximating planar waveguide. Furthermore, the propagation factors for a large number of frequencies must be evaluated to obtain a good understanding of the properties of a waveguide structure. For instance, the Brillouin diagram of Figures 4 took 420 calculations of propagation constants for different frequencies. Near resonances (intersections of modes), numerical calculations are more sensitive to error and therefore finer discretizations are necessary.

The convergence of the nonlinear solver appears to be independent of the discretization fineness and the location of the solution with respect to other solutions. Near the resonances, the iteration is as fast, only the sensitivity on the initial guess is greater.

Although Example 1 has been analyzed in many earlier papers, the results that we have for high frequencies appear to be new. Also, our calculations clearly demonstrate for the first time that due to the grating the modes do not really intersect at the Bragg conditions, but merely miss each other in the complex plane. This is shown in Figure 5 and 6. The plot for

$\mathrm{Re}(\gamma)$ and $\mathrm{Im}(\gamma)$ appear to intersect. However, using ω as a parameter, the complex eigenmodes are never equal for the same ω value.

The GADC of Example 2 has appeared before in [19], and our results for are in good general agreement, except for the attenuation coefficients which converged to much smaller values in our approach.

Figures 7-9 show the real- and imaginary part of the propagation constant as well as their separation for three different discretizations near the second Bragg. They make clear that a finer discretization must be used to resolve $\mathrm{Re}(\gamma)$ than $\mathrm{Im}(\gamma)$; in Figure 8 the results for the different meshes are so close that they are not distinguishable. Note that the intersection of the attenuation coefficient of the two modes occurs at a different value than the minimum separation of the propagation constants. It is generally accepted that the second Bragg is the minimal separation of $\mathrm{Im}(\gamma)$.

5 Conclusions

We have presented a numerical method to calculate propagation factors of periodic dielectric waveguides via DtN maps. The main advantage of this over previous approaches is that the problem is reduced to a small nonlinear eigenproblem. The interior DtN map has no closed form and must be determined numerically. Both, finite element or boundary element techniques may be used, and we found that the BEM needs less computational resources and is intrinsically faster. To obtain analytic dependence of the transverse wave number on the parameter γ we have extended the conventional branch choice. This is important to ensure convergence of the non-linear solver for guided or almost-guided modes. Our experiments show that propagation factors can be calculated in seconds to many digits of accuracy.

Branch Choice of the Complex Square Root

The sign of the square root in the transverse wave number of the semi-infinite layers is a critical isssue, since its choice determines whether the nth harmonic will be proper or improper. For a planar guide without any corrugation all modes must either move away or decay from the guiding region. Since for a planar guide the propagation constant is purely imaginary, it follows that the positive branch in (10) must be chosen.

If a small corrugation is introduced, the Floquet exponents must also undergo small changes and therefore the sign in (10) must be determined such that the transverse wave number is an analytic function of γ in the

neighborhood of the imaginary axis (with the exception of the points $\pm i\kappa$ where the function is only continuous). This reasoning leads to the conventional rule, which states that the positive branch must be chosen unless $\mathrm{Im}(k_{zn}) < -\kappa$, see, e.g., [1]. However, this rule represents an analytic continuation of the complex square root only for $\mathrm{Re}(\gamma) \leq 0$, that is, for waves that are attenuated in z. When Newton's method is used to determine a propagation factor with vanishing or very small attenuation then the iterates may jump between the right and left complex half plane before they converge to a particular value. If the function whose root has to be determined is not analytic, Newton's method will not converge and it is therefore important to find a continuation on both sides of the imaginary axis.

The function $z \mapsto \sqrt{z^2 + \kappa^2}$ has two branch cuts, one on the interval $i(\kappa, \infty)$, the other on $-i(\kappa, \infty)$. It is analytic (except for the branch points $\pm i\kappa$ where the function is only continuous) on a two-sheeted Riemann manifold which is connected at the cuts as shown in Figure 3. The upper sheet corresponds to the positive square root and proper modes, the lower sheet corresponds to the negative square root and improper modes.

Since the transverse wave numbers of the solution must be in a neighborhood of the upper imaginary axis, the matrix-Newton method is started with every k_{xn} of the two semi-infinite layers in this area. For the following matrix-Newton iterates, the sheet of a particular k_{xn} is changed whenever the straight line between the old and the new k_{xn} intersects with a branch cut.

The iteration on the Riemann manifold ensures analytic dependence on the iteration variable γ and hence convergence of the Newton scheme. If the propagation factor has converged on the left plane and if all transverse wave numbers are sufficiently separated from the branch points, the matrix-Newton iteration on the Riemann manifold will produce results that agree exactly with the conventional rule. However, near the branch points the conventional rule may not be sufficient to characterize all propagation factors.

To make this point clear, consider the neighborhoods of the branch points on the Riemann manifold. Since the branch points are identified on the upper and lower imaginary axis, the neighborhoods are always two disks on the upper and lower sheet. That implies that one of the transverse wave numbers of the corrugated waveguide can violate the conventional rule but still represent a perturbation of the planar waveguide problem. Since the iterates of the matrix-Newton method are free to move around on the Riemann surface, this method is able to locate these solutions.

References

[1] R.E. Collin and F.J. Zucker. *Antenna Theory, Part 2*, volume 7 of *Inter-University Electronics Series*. McGraw-Hill, New York, 1969.

[2] J. Jacobsen. Analytical, numerical, and experimental investigation of guided waves on a periodically strip-loaded dielectric slab. *IEEE Trans. Antennas and Propagation*, 18(3):379–388, 1970.

[3] K.C. Chang, V. Shah, and T. Tamir. Scattering and guiding of waves by dielectric gratings with arbitrary profiles. *J. Opt. Soc. Amer. A*, 70(7):804–813, July 1980.

[4] W.P. Huang. Coupled-mode theory for optical waveguides: An overview. *J. Opt. Soc. Amer. A*, 11(3):963–983, Mar. 1994.

[5] B.E. Little, W.P. Huang, and S.K. Chaudhuri. A multiple-scale analysis of grating-assisted couplers. *J. Lightwave Tech.*, 9:1254–1263, Oct. 1991.

[6] B.E. Little and H.A. Haus. A variational coupled-mode theory for periodic waveguides. *IEEE J. Quantum Elect.*, 31:2258–2264, Dec. 1995.

[7] M.G. Moharam and T.K. Gaylord. Diffraction analysis of dielectric surface-relief gratings. *J. Opt. Soc. Amer.*, 72:1385–1392, 1982.

[8] M.G. Moharam, E.B. Grann, D.A. Pommet, and T.K. Gaylord. Formulation for stable and efficient implementation of the rigorous coupled-wave analysis of binary gratings. *J. Opt. Soc. Amer. A*, 12:1068–1076, 1995.

[9] N.P.K. Cotter, T.W. Priest, and J.R. Sambles. Scattering-matrix approach to multilayer diffraction. *J. Opt. Soc. Amer. A*, 12:1097–1103, 1995.

[10] S. Peng and G.M. Morris. Efficient implementation of rigorous coupled-wave analysis for surface-relief gratings. *J. Opt. Soc. Amer. A*, 12:1087–1096, 1995.

[11] R.E. Jorgenson and R. Mittra. Efficient calculation of the free-space periodic Green's function. *IEEE Trans. Antennas and Propagation*, AP-38:633–642, 1990.

[12] A.F. Peterson. An outward-looking differential equation formulation for scattering from one-dimensional periodic diffraction gratings. *Electromagnetics*, 14:227–238, 1994.

[13] S.T. Peng, T. Tamir, and H.L. Bertoni. Theory of periodic dielectric waveguides. *IEEE Trans. Microwave Theory Tech.*, 23(1), Jan. 1975.

[14] G. Hadjicostas, J.K. Butler, G.A. Evans, N.W. Carlson, and R. Amantea. A numerical investigation of wave interactions in dielectric waveguides with periodic surface corrugations. *IEEE J. Quantum Elect.*, 26(5), May 1990.

[15] J.K. Butler, W.E. Ferguson, G.A. Evans, P. Stabile, and A. Rosen. A boundary element technique applied to the analysis of waveguides with periodic surface corrugations. *IEEE J. Quantum Elect.*, 28(7):1701–1707, 1992.

[16] J. Tausch and J. Butler. Floquet multipliers of periodic waveguides via Dirichlet-to-Neumann maps. *J. Comput. Phys.*, 159:90–102, 2000.

[17] J. L. Volakis, A. Chatterjee, and L.C. Kempel. *Finite Element Method for Electromagnetics*. IEEE Press, Piscataway, N. J., 1998.

[18] E. Allgower and K. Georg. Continuation an path following. *Acta Numerica*, pages 1–67, 1992.

[19] N.H. Sun, J.K. Butler, G.A. Evans, and L. Pang. Analysis of granting-assisted directional couplers using the Floquet-Bloch theory. *J. Lightwave Tech.*, 15(12):2301–2315, 1997.

Table captions

Table 1: Parameters for Example 1

Table 2: Parameters for Example 2

Table 3: Convergence of the propagation factor for Example 1, $\omega = \pi$, $\Lambda = 1$ μm.

Table 4: Total solution times (rounded up to the next whole second) for Example 1, $\omega = \pi$, DEC alpha 500au cpu.

Figure captions

Figure 1: Typical waveguide geometry. Light is traveling in z-direction.

Figure 2: Decomposition of the infinite strip.

Figure 3: Riemann Surface of the function $z \mapsto \sqrt{z^2 + \kappa^2}$. A neighborhood of the upper imaginary axis is shown in dark shade.

Figure 4: Brillouin Diagram (Example 1) ω versus Reγ (left) and Imγ (right), $\Lambda = 1$.

Figure 5: First Bragg in Figure 4 enlarged

Figure 6: Second Bragg in Figure 4 enlarged

Figure 7: Reγ versus grating period Λ (in μm) for various discretization parameters. GADC, two modes near resonance.

Figure 8: Imγ versus grating period Λ (in μm) for various discretization parameters. GADC, two modes near resonance.

Figure 9: Distance of the modes versus grating period Λ (in μm) for various discretization parameters. GADC, near resonance.

Figure 10: Field distributions of mode A and B. GADC, near resonance.

Region	Thickness/Λ	rel. permittivity
Ω_0	∞	1.5166
Ω_1	0.6366 + 0.4	1.7320
Ω_2	∞	1.0000

Table 1: Parameters for Example 1

Region	Thickness (μm)	rel. permittivity
Ω_0	∞	3.180
Ω_1	0.257	3.450
Ω_2	0.450 + 0.1	3.282
Ω_3	0.200 + 0.1	3.180
Ω_4	1.450	3.282
Ω_5	∞	3.180

Table 2: Parameters for Example 2

	$-\mathrm{Re}(\gamma)/\omega$ ($\times 10^{-2}$)						
h/Λ	1/4	1/8	1/16	1/32	1/64	1/128	1/256
$p=1$	3.4085	3.0962	3.0586	3.0469	3.0430	3.0427	3.0427
$p=2$	3.3769	3.0405	2.9972	2.9832	2.9787	2.9784	2.9784
$p=3$	3.3820	3.0405	2.9969	2.9832	2.9787	2.9781	2.9787
$p=4$	3.3779	3.0402	2.9963	2.9829	2.9784	2.9784	2.9784
$p=5$	3.6631	3.0405	2.9966	2.9829	2.9784	2.9781	2.9784
$p=6$	3.3785	3.0402	2.9959	2.9826	2.9784	2.9781	2.9784
$p=7$	3.6195	3.0402	2.9963	2.9826	2.9784	2.9781	2.9784
$p=8$	3.6166	3.0364	2.9959	2.9826	2.9784	2.9781	2.9784
				$\mathrm{Im}(\gamma)/\omega$			
h/Λ	1/4	1/8	1/16	1/32	1/64	1/128	1/256
$p=1$	1.578050	1.579379	1.580150	1.580485	1.580610	1.580652	1.580665
$p=2$	1.578091	1.579407	1.580170	1.580498	1.580621	1.580662	1.580675
$p=3$	1.578111	1.579424	1.580186	1.580515	1.580638	1.580679	1.580693
$p=4$	1.578115	1.579421	1.580187	1.580516	1.580638	1.580680	1.580693
$p=5$	1.578020	1.579422	1.580188	1.580517	1.580639	1.580680	1.580693
$p=6$	1.584610	1.579421	1.580188	1.580517	1.580639	1.580680	1.580693
$p=7$	1.584457	1.579423	1.580188	1.580517	1.580640	1.580680	1.580694
$p=8$	1.584459	1.579425	1.580187	1.580517	1.580640	1.580680	1.580694

Table 3: Convergence of the propagation factor for Example 1, $\omega = \pi$, $\Lambda = 1$ μm.

h/Λ	1/4	1/8	1/16	1/32	1/64	1/128	1/256
$p=1$	1	1	1	1	7	28	122
$p=2$	1	1	1	1	7	29	126
$p=3$	1	1	1	2	7	30	131
$p=4$	1	1	1	2	7	31	135
$p=5$	1	1	1	2	8	33	140
$p=6$	1	1	1	2	8	33	144
$p=7$	1	1	1	2	9	34	149
$p=8$	1	1	1	3	9	35	154

Table 4: Total solution times (rounded up to the next whole second) for Example 1, $\omega = \pi$, DEC alpha 500au cpu.

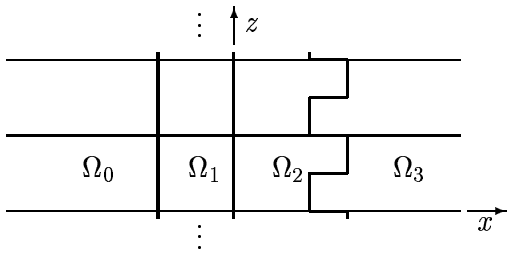

Figure 1: Typical waveguide geometry. Light is traveling in z-direction.

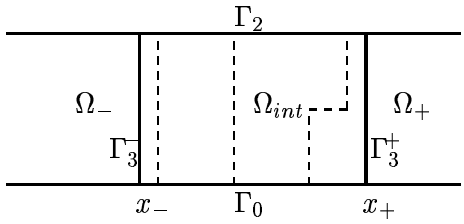

Figure 2: Decomposition of the infinite strip.

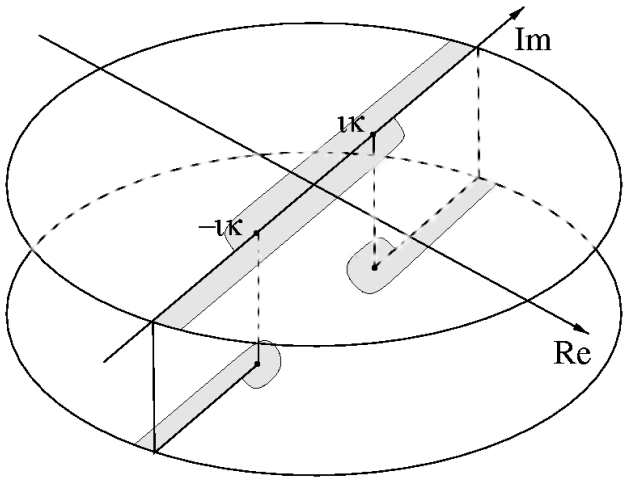

Figure 3: Riemann Surface of the function $z \mapsto \sqrt{z^2 + \kappa^2}$. A neighborhood of the upper imaginary axis is shown in dark shade.

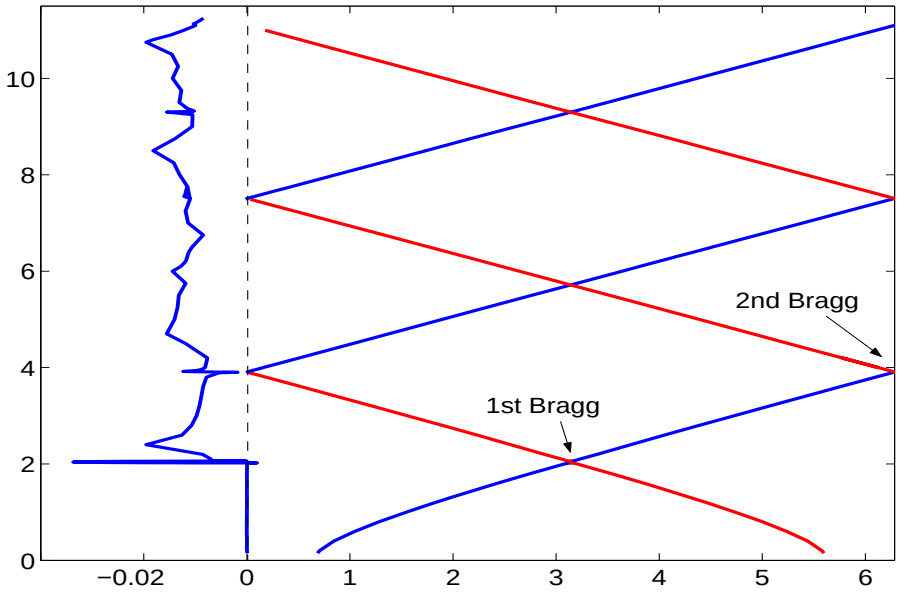

Figure 4: Brillouin Diagram (Example 1) ω versus Reγ (left) and Imγ (right), $\Lambda = 1$.

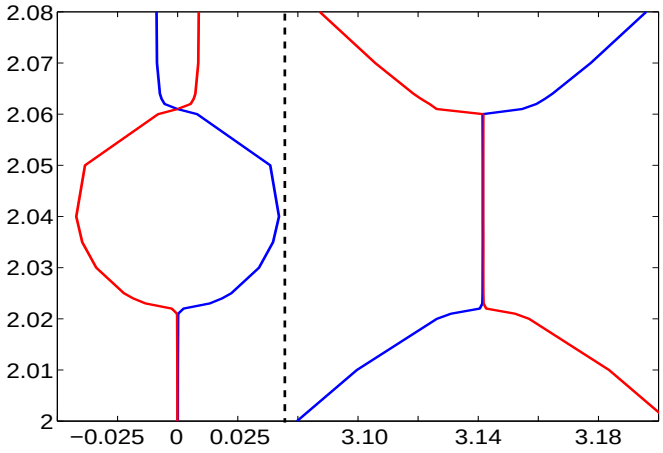

Figure 5: First Bragg in Figure 4 enlarged

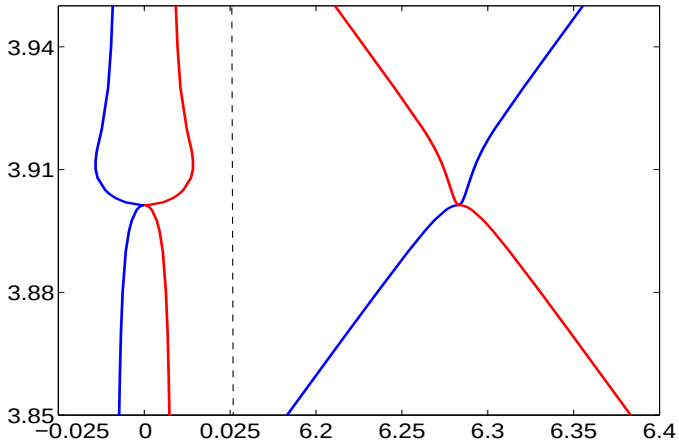

Figure 6: Second Bragg in Figure 4 enlarged

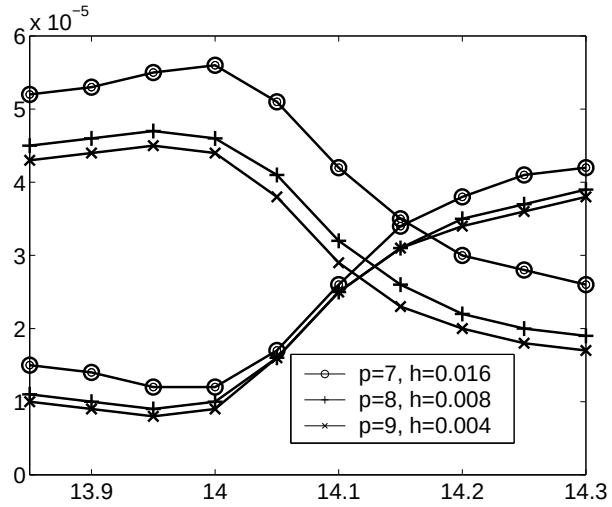

Figure 7: Reγ versus grating period Λ (in μm) for various discretization parameters. GADC, two modes near resonance.

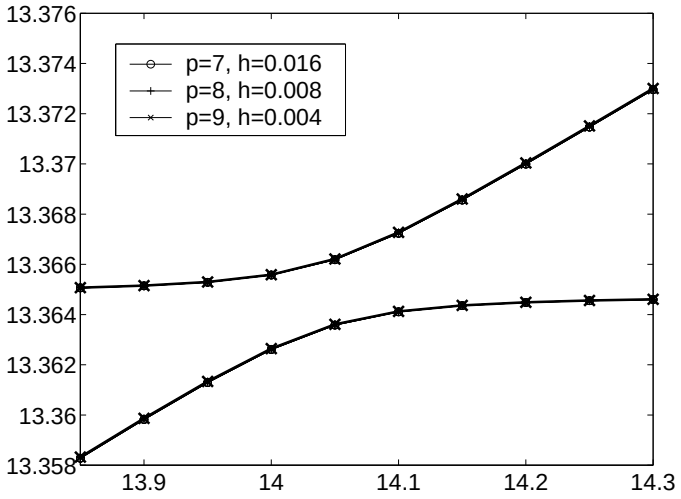

Figure 8: Imγ versus grating period Λ (in μm) for various discretization parameters. GADC, two modes near resonance.

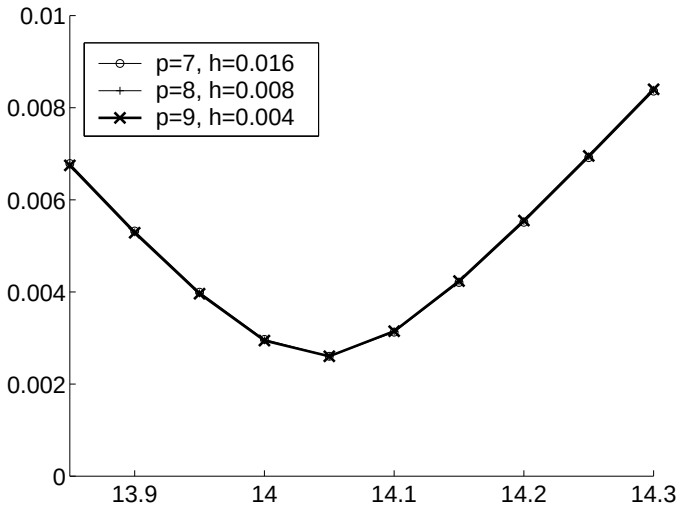

Figure 9: Distance of the modes versus grating period Λ (in μm) for various discretization parameters. GADC, near resonance.

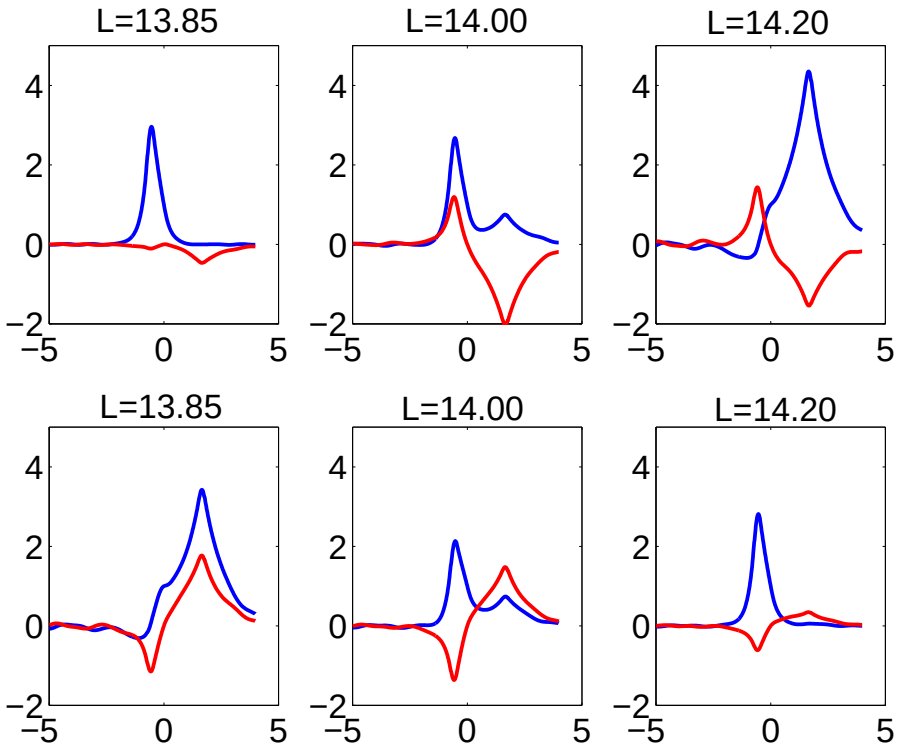

Figure 10: Field distributions of mode A and B. GADC, near resonance.